JGR Oceans

RESEARCH ARTICLE
10.1029/2022JC018909

Dynamical Controls of the Eastward Transport of Overwintering *Calanus finmarchicus* From the Lofoten Basin to the Continental Slope

Huizi Dong[1,2], Meng Zhou[1], Walker O. Smith[1,3], Baosheng Li[4], Ziyuan Hu[5], Sünnje L. Basedow[6], Frank Gaardsted[7], Zhaoru Zhang[1], and Yisen Zhong[1]

[1]School of Oceanography, Shanghai Jiao Tong University, Shanghai, China, [2]Department of Biology, Woods Hole Oceanographic Institution, Woods Hole, MA, USA, [3]Virginia Institute of Marine Science, Gloucester Point, VA, USA, [4]State Key Laboratory of Satellite Ocean Environment Dynamics, Second Institute of Oceanography MNR, Hangzhou, China, [5]Jiaozhou Bay National Marine Ecosystem Research Station, Institute of Oceanology, Chinese Academy of Sciences, Qingdao, China, [6]Department of Arctic and Marine Biology, UiT the Arctic University of Norway, Tromsø, Norway, [7]Akvaplan-niva Fram Centre, Tromsø, Norway

Key Points:

- Lagrangian Coherent Structures reveal persistent eastward transport between 600 and 1,100 m depth in winter in the northern Norwegian Sea
- There is a strong similarity between the eastward advection of the mean current and the eastward transport of diapausing *Calanus finmarchicus*
- This process is a part of the potential spatial and temporal closure of *C. finmarchicus* life histories at the basin-slope-shelf

Supporting Information:

Supporting Information may be found in the online version of this article.

Correspondence to:

M. Zhou,
meng.zhou@sjtu.edu.cn

Citation:

Dong, H., Zhou, M., Smith, W. O., Li, B., Hu, Z., Basedow, S. L., et al. (2022). Dynamical controls of the eastward transport of overwintering *Calanus finmarchicus* from the Lofoten Basin to the continental slope. *Journal of Geophysical Research: Oceans*, *127*, e2022JC018909. https://doi.org/10.1029/2022JC018909

Received 12 JUL 2022
Accepted 30 AUG 2022

Abstract Diapausing populations of *Calanus finmarchicus* at depth in the Lofoten Basin (LB) return to the continental shelf and slope off the Lofoten-Vesterålen Islands during the phytoplankton spring bloom to feed and spawn, forming surface swarms with a great abundance. To study how overwintering populations of *C. finmarchicus* move with the deep currents and return to the shelf, Lagrangian transport characteristics of particles in deep water between 2008 and 2019 were analyzed using Global Ocean Reanalysis and Simulation re-analysis data and Lagrangian Coherent Structures (LCSs). Our analyses revealed that persistent eastward transport of diapausing *C. finmarchicus* between LB and continental slope occurred mainly between 600 and 1,100 m in the Arctic Intermediate Water. The consistency of the vertical distributions of *C. finmarchicus* abundance and salinity further suggests that physical factors control the horizontal distribution of the species. Hovmöller diagrams of kinetic energy indicate that there is an eastward advection of mean current at depth. The co-occurrence between the eastward transport of LCSs and the eastward advection of the mean current provides direct evidence that the life history of *C. finmarchicus* is subjected to physical control in the Norwegian Sea.

Plain Language Summary Overwintering populations of the copepod *Calanus finmarchicus* in the Lofoten Basin (LB) are critical for maintaining its life cycle and food web in the northern Norwegian Sea. Horizontal advection and particle tracking simulation between 2008 and 2019 were performed using reanalysis data. Our analyses revealed that eastward transport between 600 and 1,100 m in the Arctic Intermediate Water below the Atlantic Water was responsible for moving *C. finmarchicus* from the LB to the continental slope. The consistency of the vertical distributions of *C. finmarchicus* and salinity further suggests that physical factors control the horizontal distribution of the species. The trend of decreasing abundance of *C. finmarchicus* from west to east in January results from the eastward transport of the species and its accumulation on the continental slope. Eastward transport from the basin to the slope is a key process in the life cycle of *C. finmarchicus* and demonstrates the importance of large-scale physical-biological interactions in Nordic Seas.

1. Introduction

The basin-slope-shelf areas in the northern Norwegian Sea are highly productive and support large populations of commercially exploited fish species such as Northeast Arctic cod (*Gadus morhua*), Norwegian spring-spawning herring (*Clupea harengus*) and capelin (*Mallotus villosu*) (Basedow et al., 2019; Zhou et al., 2009). The copepod *Calanus finmarchicus* is the main prey of these commercially harvested species, both as larvae (cod) and adults (herring and capelin) (Krumhansl et al., 2018). Populations of *C. finmarchicus* thus play a key role in linking primary producers to higher trophic levels (Melle et al., 2014; Planque, 2000). The population enters diapause in late summer, and these individuals constitute a major part of the spawning population in the following spring (Gaardsted et al., 2011; Halvorsen et al., 2003; Heath et al., 2004). This deep-water diapause strategy not only allows *C. finmarchicus* to reduce the rate of loss due to predation mortality and advective dispersal during winter, but also plays an important role in the persistence of spatial patterns of *C. finmarchicus* populations in the northern Norwegian Sea (Gaardsted et al., 2010; Hirche, 1996; Weidberg & Basedow, 2019).

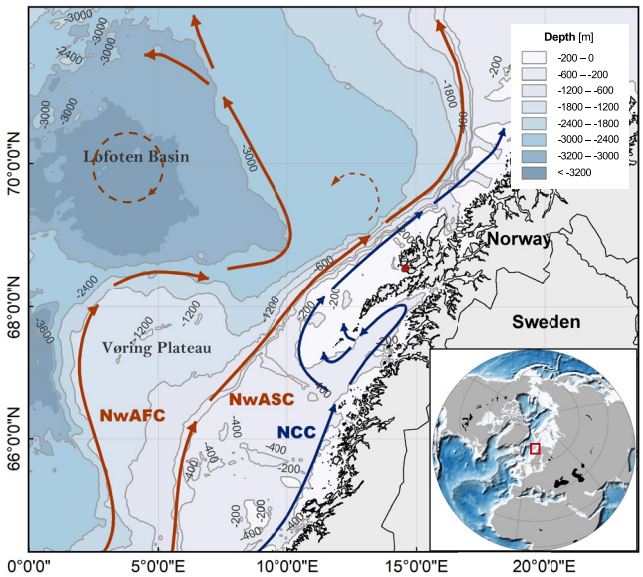

Figure 1. Bathymetry and main currents in the northern Norwegian Sea. Red arrows represent the Norwegian Atlantic Front Current and Norwegian Atlantic Slope Current, and blue arrows represent the Norwegian Coastal Current. The dashed red circle in the Lofoten Basin represents the location of Lofoten Basin Eddy. The study area is indicated by the red box in the inset.

The basin-slope-shelf topography in the northern Norwegian Sea largely determines the general circulation pattern, water mass exchange, residence time, and transport of nutrients and plankton (Espinasse et al., 2017; Slagstad & Tande, 1996; Sundby, 1984). The main water masses are of coastal and Atlantic origins (Figure 1). The Norwegian Coastal Current (NCC) flows as a buoyancy-driven and low salinity-low temperature current along the coast, bordering the parallel northeastward Norwegian Atlantic Slope Current (NwASC). The most unstable areas of the NwASC occur in the steepest part of the continental slope off the Lofoten-Vesterålen Islands (Isachsen, 2015). Due to the instability, eddies are shed from the NwASC and propagate westward to the deepest part of the Lofoten Basin (LB) (Raj et al., 2016; Yu et al., 2017). High abundances of *C. finmarchicus* have been repeatedly observed in the LB in winter (Halvorsen et al., 2003; Slagstad & Tande, 2007). It has been suggested that copepods descending from the surface of the LB to depths below the Atlantic Water (AW) may be retained in the area due to a permanent anticyclonic vortex, the Lofoten Basin Eddy (LBE) (Slagstad & Tande, 1996). However, it is unclear how *C. finmarchicus* populations are returned to the shelf in spring and the role of physical mechanisms in this movement. This process plays an important role in retaining *C. finmarchicus* populations in the northern Norwegian Sea.

In the last two decades Lagrangian techniques have been widely used to study mesoscale processes due to the increasing availability of detailed knowledge of velocity fields from Lagrangian drifters, satellite measurements and computer models (Alver et al., 2016; Hu & Zhou, 2019; Ji et al., 2012). In particular, Lagrangian Coherent Structures (LCSs) have become crucial tools for analyses of ocean flows and horizontal transport (Beron-Vera, 2010; d'Ovidio et al., 2004; Haller, 2002; Lehahn et al., 2007). Previous studies have demonstrated the ability of LCSs to analyze the spatial distribution of contaminants, primary producers and higher predators (Olascoaga et al., 2008; Scales et al., 2018; Tew Kai et al., 2009). In studies of physical-biological interactions in the Norwegian Sea, progresses have been made in understanding biomass and distributions of overwintering *C. finmarchicus* using net sampling, laser optical plankton counters (LOPC) mounted on towed undulating vehicles, video plankton recorders and drifting floats (Basedow et al., 2010; Baumgartner, 2003; Zhu et al., 2009). Coupled physical-biological models focusing on the life cycle and growth stages of *C. finmarchicus*, along with an enhanced knowledge of the complex interactions between the physical environment and the ecosystem, have improved our understanding of its life histories (Feng et al., 2018; Ji et al., 2012; Opdal & Vikebø, 2015).

Recently, the retention and cross-slope transport processes of *Calanus* spp. populations in the northern Norwegian Sea during spring seasons have been analyzed, showing that the population of *C. finmarchicus* on the Lofoten shelf is transported across the slope into the open ocean, thus contributing a large proportion of the overwintering stocks that later descends to deeper waters of the LB (Dong et al., 2021). High abundances of *C. finmarchicus* are found between 600 and 1,200 m during the overwintering period (Edvardsen et al., 2006; Gaardsted et al., 2010). However, it remains unclear how overwintering populations in deep waters move with deep currents, and in particular how the population in the LB are returned to the shelf in early spring each year. Copepods in diapause are characterized by reduced metabolism, slow development and inert behavior (Hirche, 1996; Saumweber & Durbin, 2006). The low-temperature environment of the overwintering layer reduces considerably their metabolic demand that is fueled solely by their abundant lipid stores, while avoiding predators and parasites, increasing their probability of survival in winter. This allowed us to study the horizontal transport of copepods without considering the growth, reproduction, mortality or vertical migration of the *C. finmarchicus* populations. In this study, we focus on the role of horizontal advection of the deep currents in the transport of the diapausing *C. finmarchicus* between the LB and continental slope. Employing Lagrangian advection, particle tracking simulations of LCSs and dynamical diagnosis of the kinetic energy equations, we analyze the transport processes and physical controls in this movement.

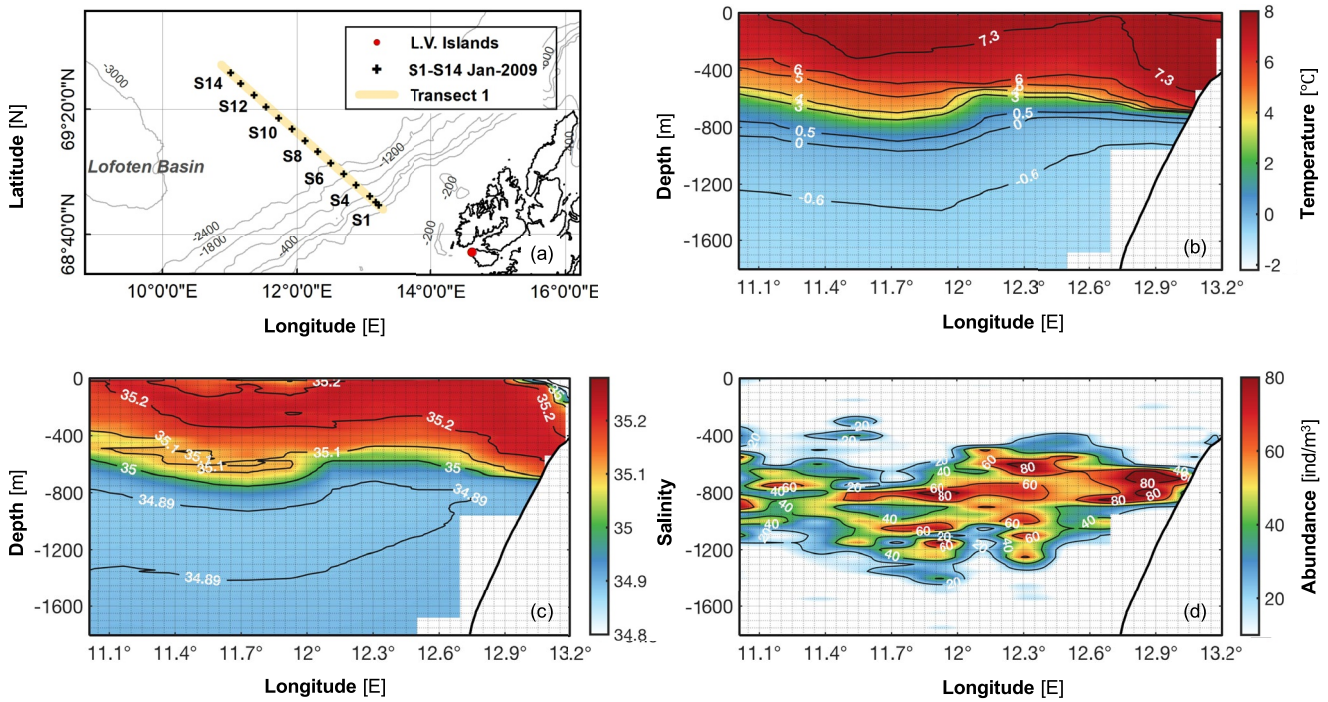

Figure 2. (a) Locations of the transects from cruise in January 2009. The red dot represents the Lofoten-Vesterålen Islands. Vertical distributions of (b) temperature, (c) salinity, and (d) *Calanus finmarchicus* abundances along Transect 1.

2. Data and Methods

2.1. Hydrographic and Zooplankton Data

Hydrographic and zooplankton data were collected off the coast of northern Norway from 24 to 30 January 2009. Depths varied from less than 200 m on the Lofoten shelf to more than 2,000 m in the eastern LB (Figure 2a). Simultaneous vertical profiles of hydrography and particle abundance were obtained at 14 stations using a CTD (SBE 911+, Seabirds Electronics, Inc., USA) and a LOPC (Brooke Ocean Technology Ltd., Canada) mounted on a rosette (Gaardsted et al., 2011). The instrument was lowered to 10 m off the bottom at stations shallower than 2,000 m and to 2,000 m at deeper stations.

Data from the LOPC provide counts and size estimates for each particle detected (Basedow et al., 2010; Gaardsted et al., 2010). The laser beam is emitted from one side of the sampling channel and is detected by a diode array on the other side (Basedow et al., 2014; Checkley et al., 2008; Herman, 1992). Details of the measurement principles and data analysis of the LOPC are well-documented (Checkley et al., 2008; Herman et al., 2004). Two types of particles are detected by the LOPC: single-element particles (SEPs) and multi-element particles (MEPs), depending on the number of diode elements that are occluded by the passing particles. Smaller particles occluding only 1–2 of the 35 diode elements are termed SEPs. These particles are automatically processed and recorded in 128 bins, with 15 μm in each size bin and ranging between 1 and 1,920 μm. Larger particles occluding three or more diode elements are termed MEPs. The digital size (DS) is used to calculate the Equivalent Spherical Diameter (ESD), which approximates the diameter of these particles (Checkley et al., 2008; Våge et al., 2014). Accordingly, an ESD of each particle from MEPs can be calculated as:

$$\mathrm{ESD}_{\mathrm{DS}} = b_1 + b_2(\mathrm{DS}) + b_3(\mathrm{DS})^2 + b_4(\mathrm{DS})^3, \quad (1)$$

where $b_1 = 0.1806059$, $b_2 = 0.00025459$, $b_3 = -1.0988 \times 10^{-9}$, and $b_4 = 9.54 \times 10^{-15}$ (Basedow et al., 2014; Gaardsted et al., 2010). To avoid the influence of bubbles and suspended particles in the surface layer, only the LOPC down-cast profiles 5 m below the surface were used for analysis. *C. finmarchicus* abundance were calculated by generating vertical averages in 50 m bins. Following Gaardsted et al. (2010), the ESD in size range of 900–1,500 μm contributed over 80% of the abundance and were used as a proxy for the overwintering *C. finmarchicus*. During the annual life cycle from egg to adult, *C. finmarchicus* pass through six nauplius

(NI-NVI) and five copepodite stages (CI-CV). We focus on the overwintering *C. finmarchicus* CIV-CV (Broms et al., 2009).

2.2. Reanalysis Data

Reanalysis data were acquired from the Global Ocean Reanalysis and Simulation (GLORYS) 12v1 product from the Copernicus Marine Environment Monitoring Service (http://marine.copernicus.eu). The reanalysis is generated using the NEMO3.1 ocean model driven at the surface by the ECMWF ERA-Interim reanalysis. It assimilates along-track altimetry sea level anomaly, satellite sea surface temperature, sea ice concentration, and in situ vertical profiles from Coriolis Ocean database for Re-Analysis v5.0 database, which includes Argo profiling floats and mooring arrays (Fedorov & Belonenko, 2020; Ferry et al., 2012). The Level-4 GLORYS 12v1 product provides global ocean circulation reanalysis at the eddy-resolving resolution of 1/12° in horizontal grids and 50 vertical levels. The use of the GLORYS 12v1 product for studying circulations in the Lofoten slope-basin areas is effective as the product was validated by the "Hydrography of the Nordic Seas, 2000–2017: A merged product" data set in previous studies (Belonenko et al., 2021; Bosse et al., 2018; Fer & Bosse, 2017). This data set consists of data from 10 glider missions, 22,117 Argo floats and 45,239 shipboard CTD profiles in the region of 61–80°N, 17°W–23°E, covering the time and space of the current study (Bosse & Fer, 2018). The GLORYS 12v1 product has also been used in previous studies for Lagrangian analysis, energy conversion in the northern Norwegian Sea, and deep-water formation in the Nordic Seas (Fedorov et al., 2021; Sgubin et al., 2017). Details of the assimilation procedures and validations of the GLORYS 12v1 are provided in Ferry et al. (2012) and Verezemskaya et al. (2021). In this study, daily velocity data at 643, 763, 902, and 1,062 m between 2008 and 2019 were used for LCSs and particle tracking simulations. These four layers were chosen because the vertical distribution of *C. finmarchicus* during the overwintering period occurs mainly between 600 and 1,200 m (Edvardsen et al., 2006). The daily temperature, salinity and velocity data at these depths in 2019 were used for dynamical diagnostics.

2.3. Lagrangian Coherent Structures (LCSs)

The LCSs were utilized to identify the spatial dynamical structures and to investigate the horizontal transport characteristics in the basin-slope areas at depth. The LCSs can be quantified by the finite-size lyapunov exponent (FSLE), which has been used to reveal the horizontal transport and track plankton populations moving with currents (d'Ovidio et al., 2015; Lévy et al., 2018; Li et al., 2022). The FSLE is computed from the time interval τ, at which two fluid particles move from an initial separation of δ_i to a final separation distance δ_f following their trajectories in the two-dimensional velocity field. At time t and position $\vec{x}$, the Lyapunov exponent λ is defined as:

$$\lambda\left(\vec{x},\, t,\, \delta_i, \delta_f\right) = \frac{1}{\tau}\log\left(\frac{\delta_f}{\delta_i}\right), \tag{2}$$

where λ is the local measure of the largest exponential separation rate of two particles. Trajectories were calculated by applying a fourth-order Runge-Kutta scheme with a time step of 3 hr. The units of FSLE are d^{-1}. δ_i determines the resolution of the Lyapunov map and δ_f affects the detection of the structures, respectively. Sensitivity analyses of LCSs for different values of δ_i and δ_f (0.01–0.08 for δ_i and 0.2–0.6 for δ_f) have been performed to find an optimal combination of these two parameters. δ_i and δ_f were set at 0.02° and 0.4° to be able to capture the mesoscale properties and to visualize the details of the LCSs in the study area. FSLE computed backward in time provides the convergence (attracting) effect, which brings initially distant water parcels to a close distance. Regions with higher values of FSLE results play an important role in controlling the horizontal exchange of water from different dynamical regions (Della Penna et al., 2015; d'Ovidio et al., 2015; Scales et al., 2018).

Horizontal advection processes are quantified by studying the stretching and contraction properties of the ocean currents and described by the LCSs (Rypina et al., 2012; Scales et al., 2018). In this study longitudinal advection were computed backward in time in the LCSs model to depict the origins and transport paths of deep water. Particles were released in different dynamical regions of the velocity fields defined by the LCSs. Trajectories of the particles were tracked backward in time for 60 days. For one particle, the longitude and latitude positions for each day were used to describe the path of this particle traveled before reaching its current position. The longitudinal advection field can be obtained by finding the position information of all particles in the study area 60 days before and mapping this longitude information to their current position. Four cases of FSLE field and longitudinal advection at 902 m for 1 December 2009, 1 January 2014, 11 December 2016, and 11 January 2019

were analyzed to provide the horizontal transport routes of water masses at depth and the different origins of the water masses reaching the continental slope. Three groups of particles were released in each of the four cases in the LCSs model to determine the origin and paths of movement of water parcels in different dynamical regions.

2.4. Particle Tracking Simulations

To trace the origin of the particles that reached the continental slope in the deep layer, four groups of particles were released at 643, 763, 902, and 1,062 m between 2008 and 2019 in the backward LCSs. Since the diapause of the overwintering *C. finmarchicus* population ends by February and *C. finmarchicus* first appears in upper layers on the Lofoten shelf from late February to early March (Dong et al., 2021; Edvardsen et al., 2006), 221 particles were released every 10 days between December and February in the 60-day LCSs simulation. The location of the particle release was chosen based on the highest EKE and the most baroclinically unstable part off the continental slope region (Isachsen, 2015; Trodahl & Isachsen, 2018). Due to the eddy activities caused by the baroclinic instability, this region has been shown to have the strongest shelf-ocean water and plankton exchange (Dong et al., 2021; Fer et al., 2020). The average number of particles contained in each grid cell of size $0.1 \times 0.2°$ over a 12-year period average number of particles (ANP) was used as an indicator of particle origin. The average number of days of particles passing through each grid cell average number of days passed (ANDP) was used to evaluate the passive transport rate of these particles.

2.5. Kinetic Energy Budget

Energetic analysis allows a quantitatively description of the conversion processes in the eddy-mean flow system and mass transport processes (Chen et al., 2014; Magalhães et al., 2017). To investigate the eddy-mean flow interactions and its influence on the *C. finmarchicus* transport at the overwintering depth, the mean kinetic energy (MKE) and eddy kinetic energy (EKE) were assessed. MKE and EKE per unit mass are defined as:

$$\mathrm{MKE} = \frac{1}{2}\left(\overline{u}^2 + \overline{v}^2\right), \tag{3}$$

$$\mathrm{EKE} = \frac{1}{2}\left(u'^2 + v'^2\right), \tag{4}$$

where the overbar denotes the monthly mean, and the prime denotes the deviation from the monthly mean. The u and v are the zonal and the meridional velocities. To further understand the dynamical mechanisms of the deep flow on the eastward transport of overwintering *C. finmarchicus*, kinetic energy diagnoses were performed to determine the processes of dynamical controls (Håvik et al., 2017; Li et al., 2020; Menna & Poulain, 2014). Hovmöller diagrams were calculated by latitudinal averaging between 68 and 71°N for the $<\partial \mathrm{MKE}/\partial t>$ and $<\partial \mathrm{EKE}/\partial t>$ terms and illustrated the propagation of these two terms. Following Kang and Curchitser (2015) and Yan et al. (2019), the MKE equation is obtained by multiplying the momentum equation by $\overline{u}$ and $\overline{v}$ and then taking the time average of their sum, which is written as:

$$\underbrace{\frac{\partial MKE}{\partial t}}_{\text{Unsteadiness}} = \underbrace{-\left[\nabla\cdot\left(\overline{\mathbf{u}'u'}\,\overline{u}\right)+\nabla\cdot\left(\overline{\mathbf{u}'v'}\,\overline{v}\right)\right]}_{\text{NL\_KE}} + \underbrace{\left(\overline{u'\mathbf{u}'}\cdot\nabla\overline{u}+\overline{v'\mathbf{u}'}\cdot\nabla\overline{v}\right)}_{-\text{BTC}}$$
$$\underbrace{-g\alpha\overline{\omega}\overline{\Delta T}}_{\text{VMHF}} \underbrace{-\nabla\cdot\left(\overline{\mathbf{u}}MKE\right)}_{\text{R\_ADV}} \underbrace{-\frac{1}{\rho_0}\nabla\cdot\left(\overline{\mathbf{u}}\overline{P_D}\right)}_{\text{R\_PRS}} \underbrace{+\overline{\mathbf{u}_h}\cdot\overline{\mathbf{F}_h}}_{\text{Forcing}} \underbrace{+\overline{\mathbf{u}_h}\cdot\overline{\mathbf{D}_h}}_{\text{Dissipation}}, \tag{5}$$

where ∇ is the three-dimensional gradient operator. The time tendency of MKE is given by the sum of the following terms:

<NL_KE>, denoting the energy gained from the nonlocal eddy kinetic energy;

<-BTC>, denoting the barotropic conversion from EKE to MKE;

<VMHF>, denoting the energy conversion from MPE due to the vertical mean heat flux, where g is the gravity constant, α is the thermal expansion coefficient of sea water, T is the temperature, and ω is the vertical velocity;

<R_ADV>, denoting the redistribution of MKE through the advection processes;

<R_PRS>, denoting the redistribution of MKE through the pressure, where P_D is the dynamical portion of pressure;

and $<\overline{\mathbf{u}_h}\cdot\overline{\mathbf{F}_h}>$ and $<\overline{\mathbf{u}_h}\cdot\overline{\mathbf{D}_h}>$ are the forcing and dissipation terms of the MKE.

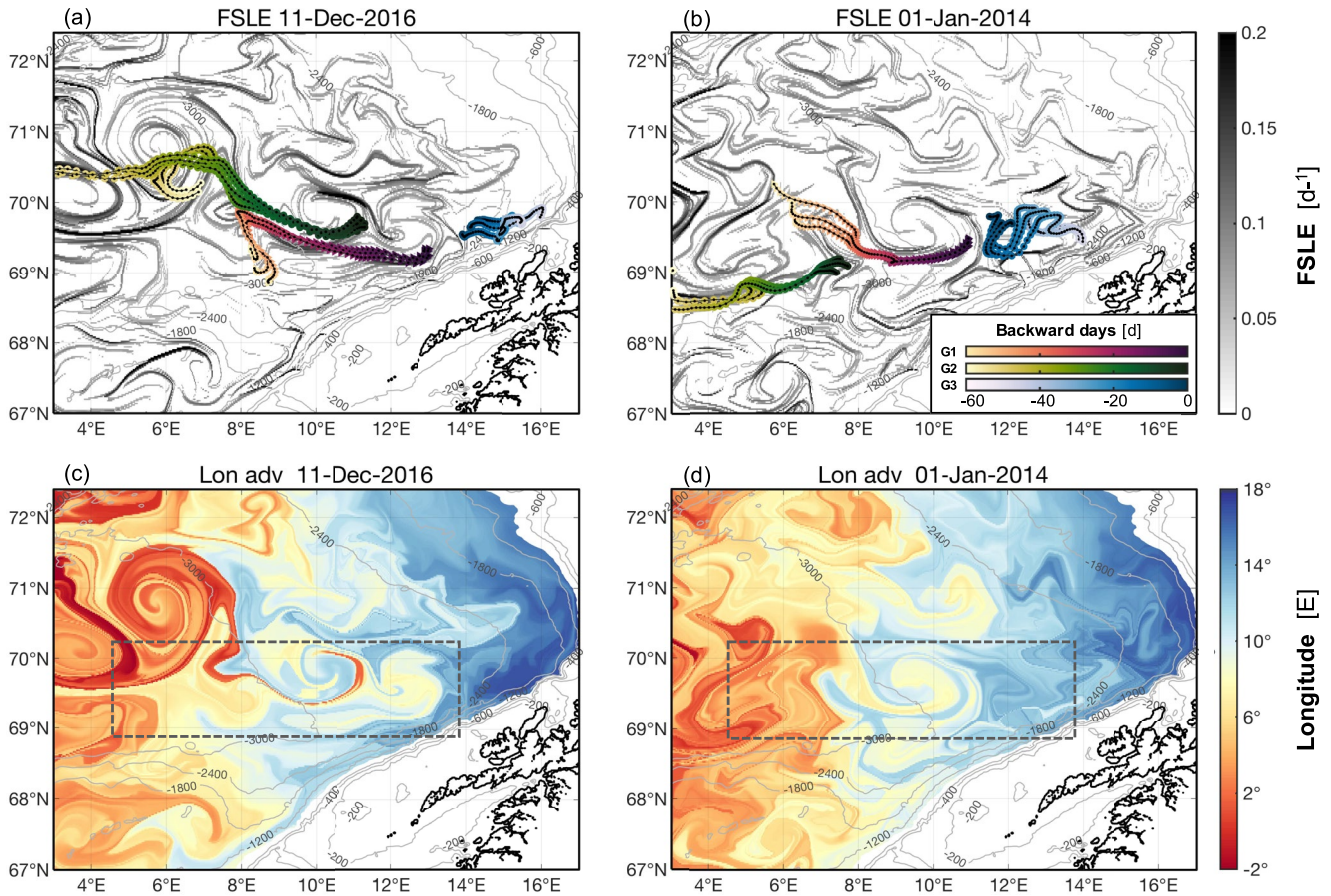

Figure 3. Paths and origins of the water parcels from Lagrangian particle tracking simulations over 60 days superposed on the Global Ocean Reanalysis and Simulation-derived finite-size lyapunov exponent (FSLE) (d^{-1}) fields at 902 m on (a) 11 December 2016, and (b) 1 January 2014. Three groups (G1, G2, and G3) of particles in (a) and (b) represent water parcels from different dynamical regions separated by the Lagrangian Coherent Structures ridges (black curves) in the FSLE field. G2 in (a) has six particles, and the other groups in (a) and all groups in (b) have three particles as representatives. The darkest color in each group indicates the location of water parcels on the day of release, (a) 11 December 2016, and (b) 1 January 2014. The lighter color indicates the earlier location in each group during the backward 60 days. The black dots and lines in each group represent the daily positions and paths of these particles. The longitudinal advections at 902 m for 60 days prior to (c) 11 December 2016, and (d) 1 January 2014. The colors in (c) and (d) represent the longitudinal positions of the 60-day origin of the water parcels. Within the areas marked by dashed boxes, a pronounced eastward transport from the LB to the slope occurs.

3. Results

3.1. Hydrographic Characteristics and *C. finmarchicus* Vertical Distributions

Temperature and salinity profiles from 24 to 30 January 2009 cruise show the well-known hydrographic characteristics of the shelf-slope-oceanic region, with the relatively warm and saline AW overlaying the colder and fresher Arctic Intermediate Water (AIW) (Figures 2a–2c). Patches of *C. finmarchicus* were distributed between 600 and 1,200 m in the AIW (Figure 2d). There was a strong correspondence between *C. finmarchicus* abundance and hydrographic structure below 600 m, especially between the copepod abundance greater than 20 ind m^{-3} and salinity less than 34.89 (Figures 2c and 2d). The distribution of *C. finmarchicus* abundance showed a pattern of lower abundance in the west and increasing abundances in the east, suggesting that the movement of the water mass might be responsible for the eastward intrusion of *C. finmarchicus* from the LB.

3.2. LCSs Advections Within the *C. finmarchicus* Overwintering Depth

Four cases of the backward FSLE and longitudinal advection fields at the depth of 902 m show the eastward transport patterns of water parcels from LB to the continental slopes in winter (Figures 3 and 4). Regions with higher values of backward FSLE indicate a strong horizontal convergence (attracting) effect which serves as a

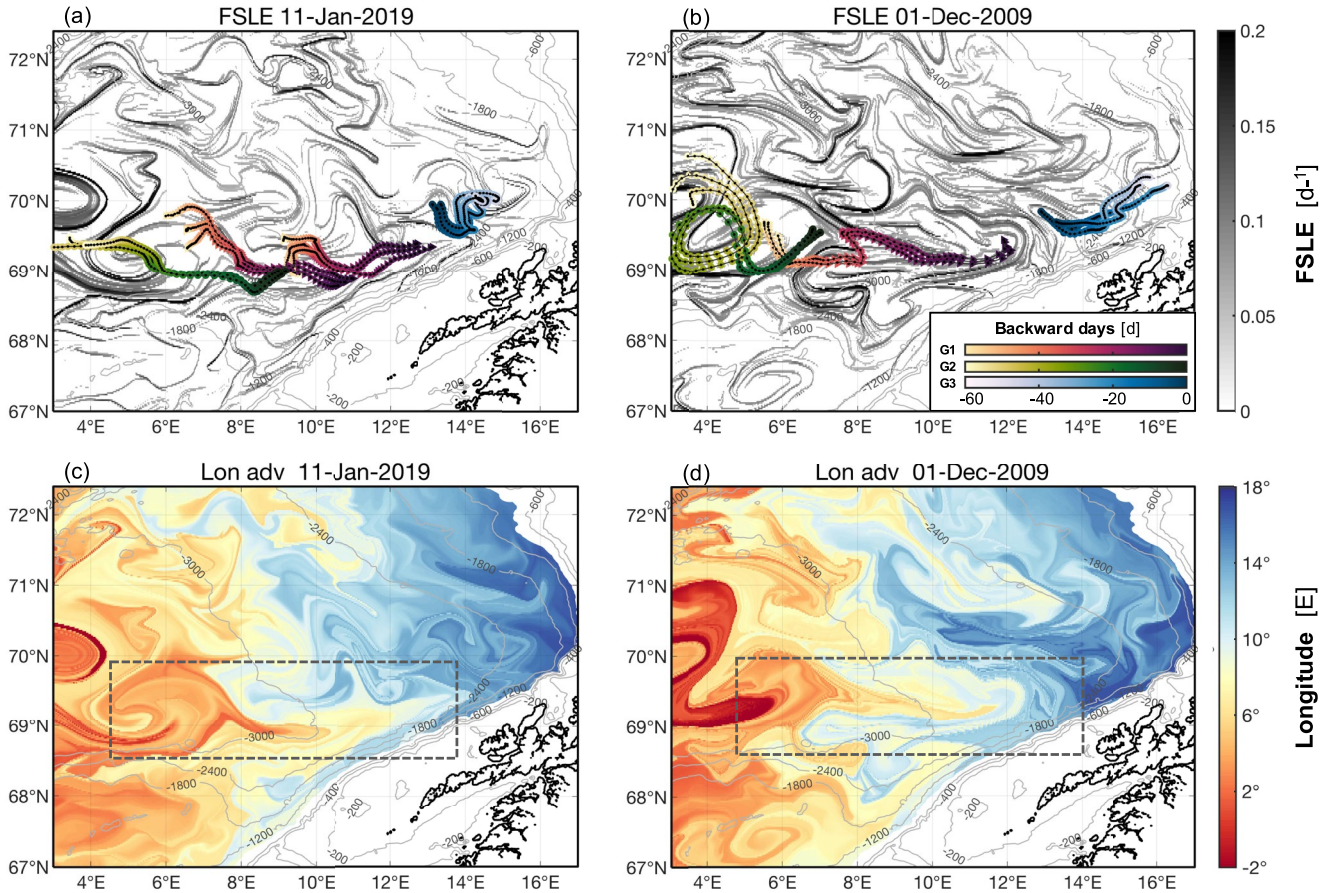

Figure 4. Paths and origins of the water parcels from Lagrangian particle tracking simulations over 60 days superposed on the Global Ocean Reanalysis and Simulation-derived finite-size lyapunov exponent (FSLE) (d^{-1}) fields at 902 m on (a) 11 January 2019, and (b) 1 December 2009. Three groups (G1, G2, and G3) of particles in (a) and (b) represent water parcels from different dynamical regions separated by the Lagrangian Coherent Structures ridges (black curves) in the FSLE field. G1 in (a) has six particles, and the other groups in (a) and all groups in (b) have three particles as representatives. The darkest color in each group indicates the location of water parcels on the day of release, (a) 11 January 2019, and (b) 1 December 2009. The lighter color indicates the earlier location in each group during the backward 60 days. The black dots and lines in each group represent the daily positions and paths of particles. The longitudinal advections at 902 m for 60 days prior to (c) 11 January 2019, and (d) 1 December 2009. The colors in (c) and (d) represent the longitudinal positions of the 60-day origin of the water parcels. Within the areas marked by dashed boxes, a pronounced eastward transport from the LB to the slope occurs.

manifold of the flows over time (Figures 3a, 3b,, and 4b). The basin-slope areas were separated into different dynamic regions by the LCSs ridges, which play a key role in the exchange of water masses and horizontal advections in the study area. In the backward simulations, particles in G1 and G2 originate from the eastern part of LB (5–9°E) and central part of LB (<5°E), respectively, and travel more than 4° to the east. Three particles in the G2 on 11 December 2016, originated in the LB and propagated eastward by more than 9° (>350 km) during the 60 days. The particles in G3 have an initial position close to G1 but belong to a distinct dynamical region than G1. They are different from the particles in G1 and G2, but come from a region near the continental slope and are transported westward.

Longitudinal advection results provide the past locations of the water parcels and the relative contributions of the water masses in different regions to the continental slope (Figures 3c, 3d,, and 4d). The flow in the area of 10–11°E, 69.3–70.2°N (red color; Figure 3c) originated 60 days ago at 0°E in the LB which has a bottom depth >3,000 m. The flow in the area of 12–13.5°E, 69–70°N (yellow color; Figure 3c) corresponds to a position around 8°E 60 days prior and illustrates its eastward intrusion into the near-slope region from the eastern LB. The longitudinal advection colored in red-yellow in the dashed boxes from 4–6°E to 10–13°E reflects the strong flow intruding eastward from the LB into the slope (Figures 3c, 3d,, and 4d).

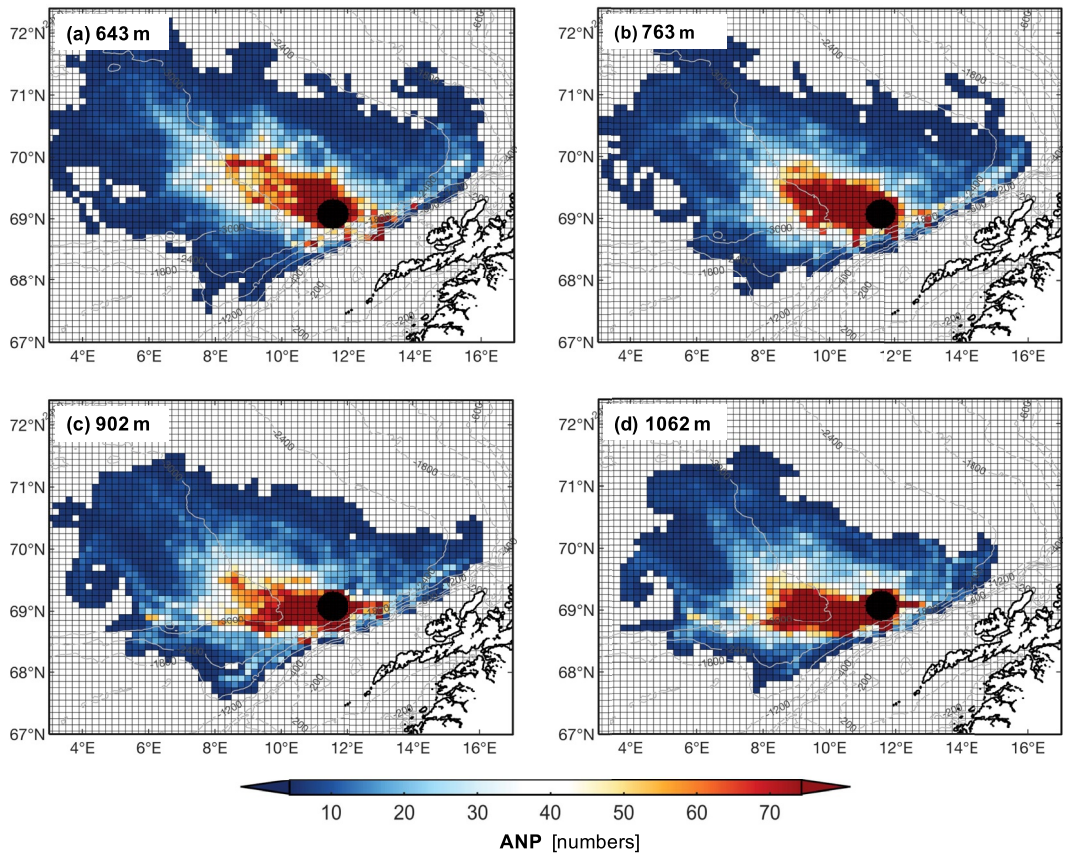

Figure 5. Average number of particles (ANP) by each grid cell for 60-day backward simulations at (a) 643, (b) 763, (c) 902, and (d) 1,062 m depth. The black dots represent the locations of particle release in the ANP.

3.3. Geographical Origin of Particles

Twelve years of backward tracking simulations showed that more than 80% of particles originating at all four depths in the LB were transported eastward toward the release region on the slope (Figures 5 and 6). Most of the particles originating from the LB entered the released region through the closest and steepest part of the slope, located at approximately 69°N, 10°E. The distributions of the ANP showed that grid cells with more than 35 particles were mostly located between 8 and 12°E (Figure 5). They converged to the released area southeastward at 643 and 763 m and eastward at 902 and 1,062 m. Grid cells with more than 25 particles (ANP) indicated that there were two main paths to the released area: one propagating southeastward along the 3,000 m isobath, and one eastward from the central LB around 69–70°N, 4–5°E. The ANDP showed that among the particles from the LB, those moving southeastward along the 3,000 m isobath moved rapidly and reached the released area in about 35–40 days (Figure 6). These 12-year particle tracking simulations further verified the existence of eastward transport processes from the LB to the near slope region at the overwintering depth of *C. finmarchicus*.

3.4. Kinetic Energy Diagnosis

A positive $<\partial MKE/\partial t>$ anomaly with values larger than 20×10^{-9} m^2 s^{-3} was observed from 4 to 12°E (~311 km) (Figure 7a). This implies that the $<\partial MKE/\partial t>$ propagated eastward with a large distance from 4°E in November to 12°E in next January (~311 km). Conversely, no significant propagation of $<\partial EKE/\partial t>$ was found (Figure 7b). Hence, $<\partial MKE/\partial t>$ played the dominant role in the eastward transport of energy. The contributions of each term to the time tendency of MKE were calculated according to Equation 5 (Figures 7c–7f). <NL_KE> and <-BTC> both showed significant eastward propagation from 3 to 12°E (~350 km) over a 3-month period (Figures 7c and 7d), similar to the propagation pattern of $<\partial MKE/\partial t>$. Although the <R_ADV> had a considerable intensity, no significant propagation eastward was observed (Figure 7e). All other terms, including <VMHF>, <R_PRS>,

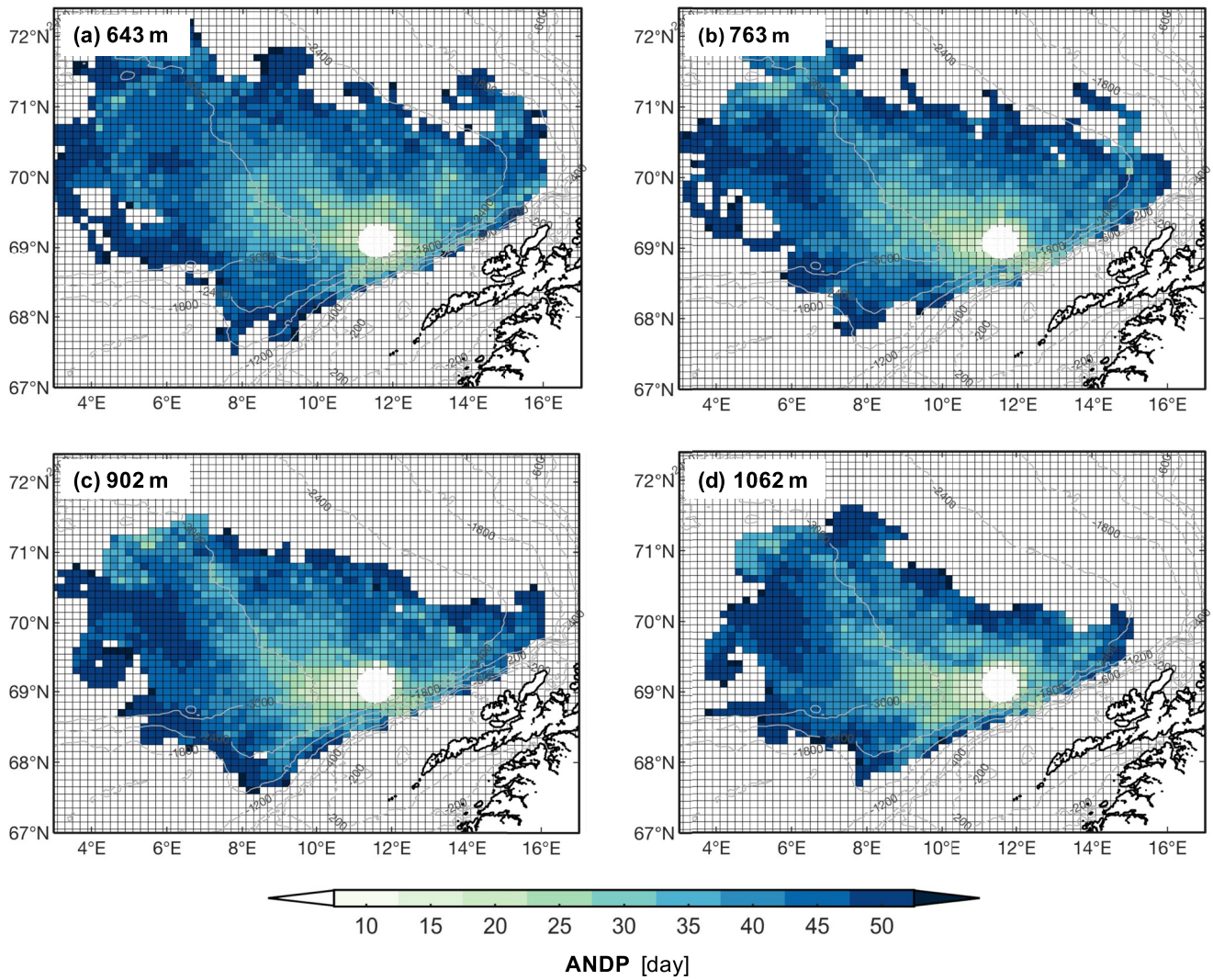

Figure 6. Average number of days passed (ANDP) by each grid cell for 60-day backward simulations at (a) 643, (b) 763, (c) 902, and (d) 1,062 m depth. The white dots represent the locations of particle release in the ANDP.

<Forcing>, and <Dissipation>, are minor, so they were all placed in residual term <RTs>. It was seen that the residual term is a sink for <∂MKE/∂t> (Figure 7f). Therefore, <NL_KE> and <-BTC> dominated the changes of MKE. The pronounced positive <NL_KE> anomaly indicated that the nonlocal eddy kinetic fields provides one part of energy for <∂MKE/∂t> during the propagation from 3 to 12°E (~350 km). The positive value of the <-BTC> indicated that the absorption of EKE into the mean flow provides another part of the energy during the eastward transport processes. In short, nonlocal kinetic energy feeding and energy conversion from EKE to MKE combine to maintain the stable eastward propagation of energy from LB to the continental slope at overwintering depths from November to January.

4. Discussion

4.1. The Source of the Surface Population in Spring

The early spring distribution of *C. finmarchicus* in the Lofoten area reflects the re-occurrence of the copepods on the shelf immediately after seasonal migration from deep diapause habitats where developmental stages CIV and CV reside for overwintering (Broms et al., 2009; Head et al., 2013). Several areas in the northern Norwegian Sea are considered to be habitats of high winter abundance of *C. finmarchicus*, such as the Faroe-Shetland Channel, the Norwegian Trench, nearby deep Norwegian fjords, and the LB (Espinasse et al., 2016; Halvorsen

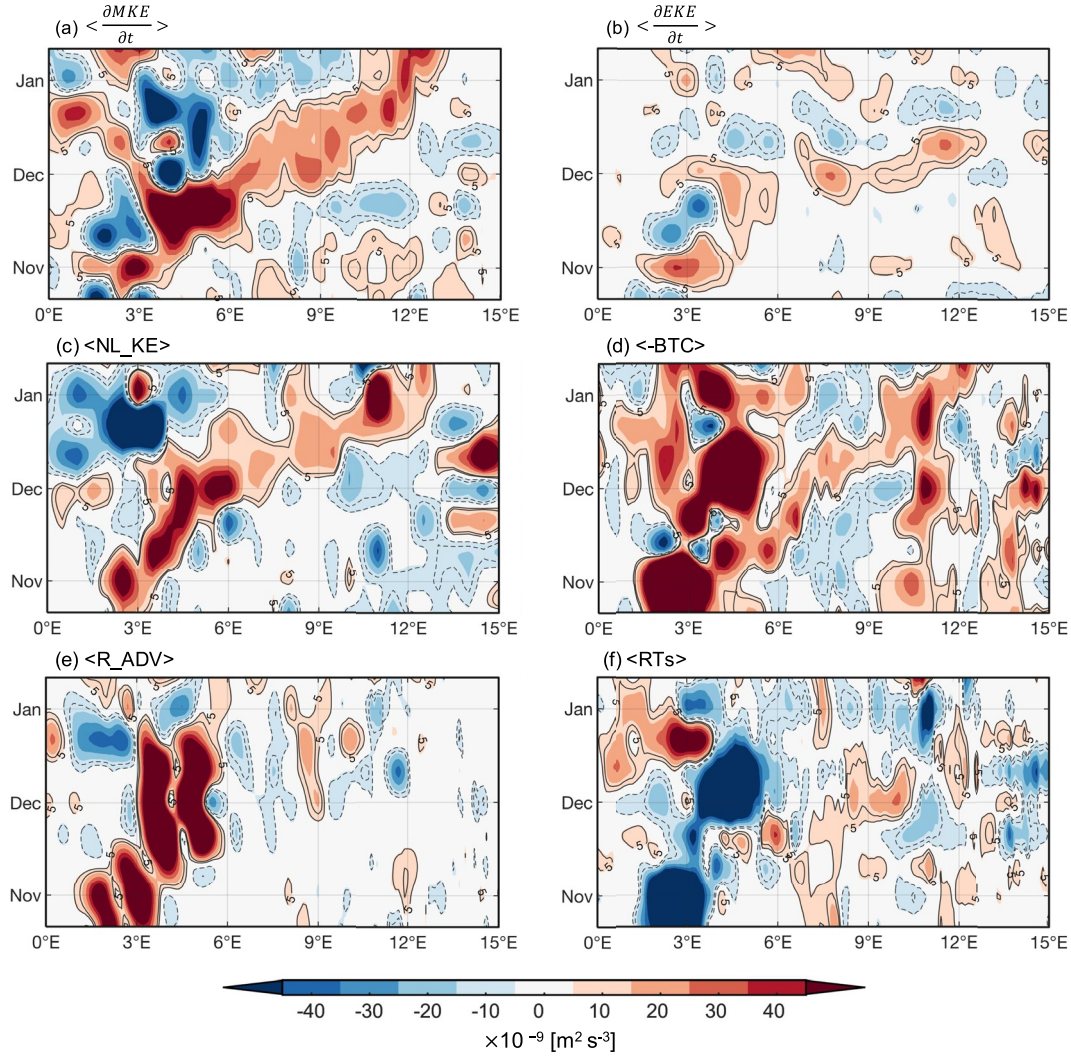

Figure 7. Hovmöller diagrams of the composite terms in Equation 5 for (a) <∂MKE/∂t>, (b) <∂EKE/∂t>, (c) <NL_KE>, (d) <-BTC>, (e) <R_ADV> and (f) the <RTs> between 600 and 1,100 m. The x-axis represents the longitude on the latitudinal average of 68–71°N. The time range of y-axis is from November 2018 to January 2019. <NL_KE>, <-BTC> and < R_ADV > are defined in Equation 5. <RTs> represents all other residual terms $<-g\alpha\overline{\omega}\overline{\Delta T}-\frac{1}{\rho_0}\nabla\cdot\left(\overline{\mathbf{u}}\overline{P_D}\right)+\overline{\mathbf{u}_h}\cdot\overline{\mathbf{F}_h}+\overline{\mathbf{u}_h}\cdot\overline{\mathbf{D}_h}>$.

et al., 2003; Opdal & Vikebø, 2015). *C. finmarchicus* that originates from the Faroe-Shetland Channel or the Norwegian Trench can easily be transported northward by both the NwASC and the NCC (Heath et al., 2004). The fjord circulation can also bring them onto the shelf once their dormancy ends (Espinasse et al., 2016). Opdal and Vikebø (2015) modeled the pathways of copepods in different areas of the northern Norwegian Sea, and found that the population on the continental shelf area north of 66°N originated mainly from the LB. Our study simulated the origin of the population at 600–1,100 m depth over 12 winters and found that more than 80% of the particles were from the LB in the region of 11–12°E, 68.8–69.4°N. Further sampling analyses of overwintering populations are needed to determine the importance of each source as a seed population of *C. finmarchicus*.

4.2. Controlling Factors for Eastward Transport of Overwintering *C. finmarchicus*

The results of the LCSs advection at depths indicate an eastward transport pattern from the LB to the continental slope (Figures 3 and 4). Particle tracking simulations were run for 12 years to demonstrate the stability of the source in the LB, and the route of these particles reached the continental slope within 60 days (Figures 5 and 6). *C. finmarchicus* in diapause within the LB was advected and traveled eastward, then eventually arrived at the

slope before February. Edvardsen et al. (2006) also found that the abundance of *C. finmarchicus* was lower in the western region in January. Previous studies have reported that the attracting LCSs could be places for prey accumulation, as the horizontal currents will transport the passively advected population near the LCSs ridges (d'Ovidio et al., 2015; Tew Kai et al., 2009). Due to the transport barrier effect of the attracting LCSs, the population will accumulate on the LCSs ridges without crossing the structures to other dynamical regions. This is the reason for the accumulation of high copepod biomass on the continental slope after the eastward intrusion of *C. finmarchicus* from the LB. The deep-water diapause strategy allows us to study the horizontal transport of overwintering *C. finmarchicus*, regardless of biological factors such as growth, reproduction and mortality. Physical drivers are the most important factor in the eastward transport of *C. finmarchicus* during winter.

4.3. Dynamical Mechanisms of the Transport Between Basin and Slope

The LB is characterized by strong mesoscale eddy activities and the permanent LBE (Raj et al., 2016; Søiland et al., 2016). Eddies that are shed from the NwASC propagate westward, sustaining the LBE and carrying warm and salty AW into the LB (Ghaffari et al., 2018; Søiland & Rossby, 2013). This process plays an important role in driving the cross-slope transport of *C. finmarchicus* and their large-scale surface distribution in spring (Dong et al., 2021). When the copepods begin to descend from the surface to their overwintering habitat in late summer, the LB serves as one of the major biological reservoirs. The strongly nonlinear LBE separates the interior water from its surroundings through a closed potential vorticity profile, which allows the overwintering species to be trapped there (Bosse et al., 2019; Early et al., 2011; Zhang et al., 2014). Previous studies have also reported enhanced lateral exchange and mixing between the LB and its surroundings during winter (Bosse et al., 2019); this suggests that *C. finmarchicus* may leave the LB before the end of the overwintering period. The longitudinal advection computations have estimated the potential sources and periods for *C. finmarchicus* concentrated at the slope region (Figures 3 and 4). The propagation of $<\partial \mathrm{MKE}/\partial t>$ at depth is the key dynamical control that enables these diapausing *C. finmarchicus* that leave the LB to transport eastward and be able to reach the continental slope by early February.

4.4. Potential Mechanisms of Intrusion of *C. finmarchicus* Onto the Lofoten Shelf

The lipid reserves of wax esters of overwintering *C. finmarchicus* allow the copepods to migrate vertically due to their higher thermal expansion and compressibility than seawater (Heath, 1999; Saumweber & Durbin, 2006; Visser & Jónasdóttir, 1999). Thus, copepods that are neutrally buoyant at low temperatures in the deep AIW can become positively buoyant when they enter the warm AW. Previous studies have reported that copepods starting from neutrally buoyant depths require only a small energy expenditure to initiate a buoyancy-assisted ascent to the surface (Visser & Jónasdóttir, 1999).

The eastbound movements of the AW at depth that can transport the copepods may occur as a counter current when the low salinity NCW spreads westward offshore (Pedersen et al., 2001). Wind-induced seasonal lateral displacement of the NCW plays a potential role in driving the intrusion of *C. finmarchicus* onto the shelf (Helland-Hansen & Nansen, 1909; Sætre, 1999). During winter, cyclones cause southwesterly winds that lead to conditions favorable for downwelling in coastal areas. This causes the wedge-shaped NCW to become deeper and narrower. After winter, cyclones and winds decrease and downwelling becomes less frequent, so the NCW becomes shallower, which might lead to an eastward movement of AW at depth (Skagseth et al., 2011).

The eastward expansion of less dense surface waters of the NCW might also aggregate ascending copepods on the shelf when they migrate into these NCW surface waters after overwintering (Weidberg et al., 2022). In this process, the vertical migration of copepods is essential; therefore, the intrusion onto the shelf in spring is likely a combination of physical processes (aggregation at shelf break, eastward expansion of NCW, eddies) and biological drivers (surface migration of copepods).

4.5. The Spatial Distributions of *C. finmarchicus* Throughout Their Life Cycle at the Basin Scale

The existence of persistent overwintering habitats at LB and the transport routes between LB and Lofoten shelf suggest that there may be a potential regular spatial and temporal closure of the life cycle of *C. finmarchicus* (Edvardsen et al., 2006; Heath et al., 2004). Therefore, the life cycle of *C. finmarchicus* in the basin-slope-shelf areas can be summarized as four main phases in four specific spatial regimes linked by horizontal transport or vertical movement (Figure 8): (Phase A) Diapause in the LB as CIV and CV copepodites followed by transport eastward from LB to the continental slope; (Phase B) Aggregation and accumulation at the slope and maturation

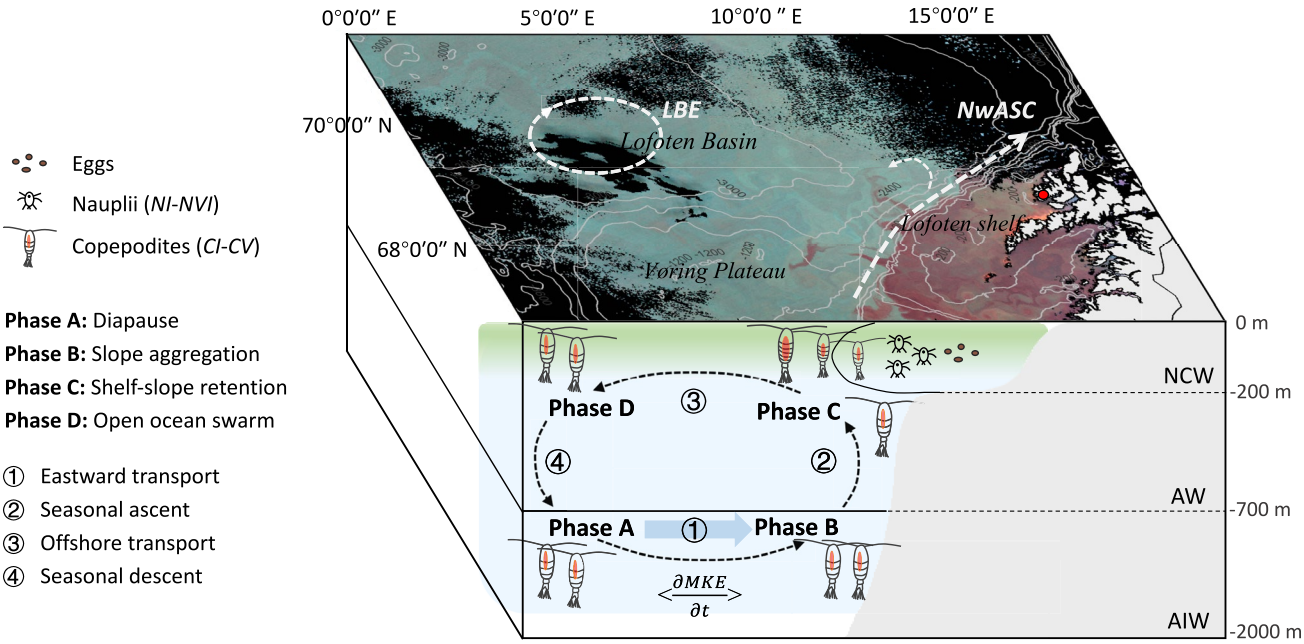

Figure 8. Conceptual diagram of the seasonal life cycle of the copepod *Calanus finmarchicus* in the basin-slope-shelf areas in the northern Norwegian Sea. The surface is an RGB composite image from ocean color remote sensing on 23 April 2014 (Phase C). The red areas on the Lofoten shelf represent areas with the high abundance of *C. finmarchicus* and the blue-green area off the Lofoten shelf represent the open ocean with low abundances of the copepod (see Text S1 in Supporting Information S1). The red dot in the ocean color image represents the Lofoten-Vesterålen Islands, and the dashed white line and dashed white cycle represent the Norwegian Atlantic Slope Current and Lofoten Basin Eddy, respectively. During Phases C and D in spring and summer, the copepods feed on phytoplankton in the upper layer, which is illustrated by the green shading.

into adults followed by ascent onto the shelf; (Phase C) Shelf retention due to transport barriers during which time reproduction occurs followed by transport across the slope to the deep waters; (Phase D) open ocean near-surface swarm period and accumulation of storage lipids in the LB followed by descent into the overwintering habitat re-entry into Phase A (diapause).

5. Conclusions

This study demonstrates the importance of horizontal transport of overwintering populations from the LB for *C. finmarchicus* shelf populations and further establishes the region as a key source for the *C. finmarchicus* population on the Lofoten shelf in early spring. The stability of eastward transport at 600–1,100 m in AIW during winter can play a significant role in transporting diapausing *C. finmarchicus* to the continental slope each year. This process is a part of the potential regular spatial and temporal closure of *C. finmarchicus* population at the basin-slope-shelf areas in the northern Norwegian Sea.

The eastward propagation of the MKE is the main dynamical control that results in *C. finmarchicus* overwintering in the LB to reach the continental slope by early February. Further dynamical diagnostics indicate that nonlocal kinetic energy feeding and energy conversion from eddy to mean currents produce a stable eastward transport mechanism for *C. finmarchicus* from LB to the continental slope at overwintering depths.

Conflict of Interest

The authors declare no conflicts of interest relevant to this study.

Data Availability Statement

The reanalysis product GLORYS 12v1 (GLOBAL_REANALYSIS_PHY_001_030) is provided by Copernicus Marine Environmental Monitoring Service (https://resources.marine.copernicus.eu/product-detail/GLOBAL_MULTIYEAR_PHY_001_030/DATA-ACCESS). The ocean color remote sensing data was provided by the Ocean Biology Processing Group (https://oceancolor.gsfc.nasa.gov). The observational data are achieved at

https://figshare.com/articles/dataset/2009_LOPC/20684149. The processed observational and model data are achieved at https://figshare.com/articles/dataset/Processed_Data/20691913.

Acknowledgments
This work is supported by the Sino-Norway Collaborative STRESSOR Project, funded by the Natural Science Foundation of China (NSFC Grant No. 41861134040) and the Research Council of Norway (RCN Grant No. 287043). This study is also supported by the NSFC Special Program (Grant No. 41941008), and the Shanghai Frontiers Science Center of Polar Science (SCOPS). The authors acknowledge the Captain and crew of *R/V Helmer Hanssen*. We would like to thank Professor Francesco d'Ovidio for support of the LCS. A portion of this work was completed while H. Dong was a guest student at the Woods Hole Oceanographic Institution, collaborating with Carin Ashjian and Rubao Ji; their contributions and suggestions are warmly acknowledged. We thank Huijie Xue and Zhongping Lee for valuable comments. We also thank Shengyang Fang for valuable comments and language revisions.

References

Alver, M. O., Broch, O. J., Melle, W., Bagøien, E., & Slagstad, D. (2016). Validation of an Eulerian population model for the marine copepod *Calanus finmarchicus* in the Norwegian Sea. *Journal of Marine Systems*, *160*, 81–93. https://doi.org/10.1016/J.JMARSYS.2016.04.004

Basedow, S. L., McKee, D., Lefering, I., Gislason, A., Daase, M., Trudnowska, E., et al. (2019). Remote sensing of zooplankton swarms. *Scientific Reports*, *9*(1), 686. https://doi.org/10.1038/S41598-018-37129-X

Basedow, S. L., Tande, K. S., & Stige, L. C. (2010). Habitat selection by a marine copepod during the productive season in the Subarctic. *Marine Ecology Progress Series*, *416*, 165–178. https://doi.org/10.3354/MEPS08754

Basedow, S. L., Zhou, M., & Tande, K. S. (2014). Secondary production at the polar front, Barents sea, August 2007. *Journal of Marine Systems*, *130*, 147–159. https://doi.org/10.1016/J.JMARSYS.2013.07.015

Baumgartner, M. F. (2003). Comparisons of *Calanus finmarchicus* fifth copepodite abundance estimates from nets and an optical plankton counter. *Journal of Plankton Research*, *25*(7), 855–868. https://doi.org/10.1093/PLANKT/25.7.855

Belonenko, T. V., Zinchenko, V. A., Fedorov, A. M., Budyansky, M. V., Prants, S. V., & Uleysky, M. Y. (2021). Interaction of the Lofoten vortex with a satellite cyclone. *Pure and Applied Geophysics*, *178*(1), 287–300. https://doi.org/10.1007/S00024-020-02647-1

Beron-Vera, F. J. (2010). Mixing by low- and high-resolution surface geostrophic currents. *Journal of Geophysical Research*, *115*(C10), C10027. https://doi.org/10.1029/2009JC006006

Bosse, A., & Fer, I. (2018). Hydrography of the Nordic Seas, 2000-2017: A merged product. Retrieved from https://urldefense.com/v3/__%2010.21335/NMDC-1131411242__;!!N11eV2iwtfs!pivwkVAc43l5DwDBal-gRIEj9r57k_v_o0KIzWTLUtleZTXk_HldyUTuTvMrhuVTbkr7s-jUhfNj9Kw-5jXKiH9g$

Bosse, A., Fer, I., Lilly, J. M., & Søiland, H. (2019). Dynamical controls on the longevity of a non-linear vortex: The case of the Lofoten Basin Eddy. *Scientific Reports*, *9*, 1–13. https://doi.org/10.1038/S41598-019-49599-8

Bosse, A., Fer, I., Søiland, H., & Rossby, T. (2018). Atlantic water transformation along its poleward pathway across the Nordic Seas. *Journal of Geophysical Research: Oceans*, *123*(9), 6428–6448. https://doi.org/10.1029/2018JC014147

Broms, C., Melle, W., & Kaartvedt, S. (2009). Oceanic distribution and life cycle of *Calanus* species in the Norwegian Sea and adjacent waters. *Deep-Sea Research Part II: Tropical Studies in Oceanography*, *56*(21–22), 1910–1921. https://doi.org/10.1016/J.DSR2.2008.11.005

Checkley, D. M., Davis, R. E., Herman, A. W., Jackson, G. A., Beanlands, B., & Regier, L. A. (2008). Assessing plankton and other particles in situ with the SOLOPC. *Limnology & Oceanography*, *53*(5part2), 2123–2136. https://doi.org/10.4319/LO.2008.53.5_PART_2.2123

Chen, R., Flierl, G. R., & Wunsch, C. (2014). A description of local and nonlocal eddy–mean flow interaction in a global eddy permitting state estimate. *Journal of Physical Oceanography*, *44*(9), 2336–2352. https://doi.org/10.1175/JPO-D-14-0009.1

Della Penna, A., De Monte, S., Kestenare, E., Guinet, C., & d'Ovidio, F. (2015). Quasi-planktonic behavior of foraging top marine predators. *Scientific Reports*, *5*, 1–10. https://doi.org/10.1038/SREP18063

Dong, H., Zhou, M., Hu, Z., Zhang, Z., Zhong, Y., Basedow, S. L., & Smith, W. O. (2021). Transport barriers and the retention of *Calanus finmarchicus* on the Lofoten shelf in early spring. *Journal of Geophysical Research: Oceans*, *126*(8), e2021JC017408. https://doi.org/10.1029/2021JC017408

d'Ovidio, F., Della Penna, A., Trull, T. W., Nencioli, F., Pujol, M. I., Rio, M. H., et al. (2015). The biogeochemical structuring role of horizontal stirring: Lagrangian perspectives on iron delivery downstream of the Kerguelen plateau. *Biogeosciences*, *12*, 5567–5581. https://doi.org/10.5194/BG-12-5567-2015

d'Ovidio, F., Fernández, V., Hernández-García, E., & López, C. (2004). Mixing structures in the Mediterranean Sea from finite-size Lyapunov exponents. *Geophysical Research Letters*, *31*(17), L17203. https://doi.org/10.1029/2004GL020328

Early, J. J., Samelson, R. M., & Chelton, D. B. (2011). The evolution and propagation of quasigeostrophic ocean eddies. *Journal of Physical Oceanography*, *41*(8), 1535–1555. https://doi.org/10.1175/2011JPO4601.1

Edvardsen, A., Pedersen, J. M., Slagstad, D., Semenova, T., & Timonin, A. (2006). Distribution of overwintering *Calanus* in the North Norwegian Sea. *Ocean Science*, *2*, 87–96. https://doi.org/10.5194/OS-2-87-2006

Espinasse, B., Basedow, S. L., Tverberg, V., Hattermann, T., & Eiane, K. (2016). A major *Calanus finmarchicus* overwintering population inside a deep fjord in northern Norway: Implications for cod larvae recruitment success. *Journal of Plankton Research*, *38*(3), 604–609. https://doi.org/10.1093/PLANKT/FBW024

Espinasse, B., Tverberg, V., Basedow, S. L., Hattermann, T., Nøst, O. A., Albretsen, J., et al. (2017). Mechanisms regulating inter-annual variability in zooplankton advection over the Lofoten shelf, implications for cod larvae survival. *Fisheries Oceanography*, *26*(3), 299–315. https://doi.org/10.1111/FOG.12193

Fedorov, A. M., & Belonenko, T. V. (2020). Interaction of mesoscale vortices in the Lofoten Basin based on the GLORYS database. *Russian Journal of Earth Sciences*, *20*(2), ES2002. https://doi.org/10.2205/2020ES000694

Fedorov, A. M., Raj, R. P., Belonenko, T. V., Novoselova, E. V., Bashmachnikov, I. L., Johannessen, J. A., & Pettersson, L. H. (2021). Extreme convective events in the Lofoten Basin. *Pure and Applied Geophysics*, *178*(6), 2379–2391. https://doi.org/10.1007/S00024-021-02749-4

Feng, Z., Ji, R., Ashjian, C., Campbell, R., & Zhang, J. (2018). Biogeographic responses of the copepod *Calanus glacialis* to a changing Arctic marine environment. *Global Change Biology*, *24*(1), e159–e170. https://doi.org/10.1111/GCB.13890

Fer, I., & Bosse, A. (2017). *Seaglider missions in the Lofoten Basin of the Norwegian Sea, 2012–2015*. (Technical report). Geophysical Institute, University of Bergen. https://doi.org/10.21335/NMDC-UIB.2017-0001 .

Fer, I., Bosse, A., & Dugstad, J. (2020). Norwegian Atlantic slope current along the Lofoten Escarpment. *Ocean Science*, *16*(3), 685–701. https://doi.org/10.5194/OS-16-685-2020

Ferry, N., Parent, L., Garric, G., Bricaud, C., Testut, C. E., Le Galloudec, O., et al. (2012). GLORYS2V1 global ocean reanalysis of the altimetric era (1992–2009) at meso scale. *Mercator Ocean–Quaterly Newsletter*, *44*, 29–39.

Gaardsted, F., Tande, K. S., & Pedersen, O.-P. (2011). Vertical distribution of overwintering *Calanus finmarchicus* in the NE Norwegian Sea in relation to hydrography. *Journal of Plankton Research*, *33*(10), 1477–1486. https://doi.org/10.1093/PLANKT/FBR042

Gaardsted, F., Zhou, M., Pavlov, V., Morozov, A., & Tande, K. S. (2010). Mesoscale distribution and advection of overwintering *Calanus finmarchicus* off the shelf of northern Norway. *Deep-Sea Research Part I: Oceanographic Research Papers*, *57*(11), 1465–1473. https://doi.org/10.1016/J.DSR.2010.07.003

Ghaffari, P., Isachsen, P. E., Nøst, O. A., & Weber, J. E. (2018). The influence of topography on the stability of the Norwegian Atlantic Current off northern Norway. *Journal of Physical Oceanography*, *48*(11), 2761–2777. https://doi.org/10.1175/JPO-D-17-0235.1

Håvik, L., Våge, K., Pickart, R. S., Harden, B., von Appen, W.-J., Jónsson, S., & Østerhus, S. (2017). Structure and variability of the shelfbreak East Greenland Current north of Denmark Strait. *Journal of Physical Oceanography*, *47*(10), 2631–2646. https://doi.org/10.1175/JPO-D-17-0062.1

Haller, G. (2002). Lagrangian coherent structures from approximate velocity data. *Physics of Fluids*, *14*(6), 1851–1861. https://doi.org/10.1063/1.1477449

Halvorsen, E., Tande, K. S., Edvardsen, A., Slagstad, D., & Pedersen, O. P. (2003). Habitat selection of overwintering *Calanus finmarchicus* in the NE Norwegian Sea and shelf waters off Northern Norway in 2000–02. *Fisheries Oceanography*, *12*(4–5), 339–351. https://doi.org/10.1046/J.1365-2419.2003.00255.X

Head, E. J. H., Melle, W., Pepin, P., Bagøien, E., & Broms, C. (2013). On the ecology of *Calanus finmarchicus* in the Subarctic North Atlantic: A comparison of population dynamics and environmental conditions in areas of the Labrador Sea-Labrador/Newfoundland Shelf and Norwegian Sea Atlantic and Coastal Waters. *Progress in Oceanography*, *114*, 46–63. https://doi.org/10.1016/J.POCEAN.2013.05.004

Heath, M. R. (1999). The ascent migration of *Calanus finmarchicus* from overwintering depths in the Faroe-Shetland Channel. *Fisheries Oceanography*, *8*, 84–99. https://doi.org/10.1046/J.1365-2419.1999.00013.X

Heath, M. R., Boyle, P. R., Gislason, A., Gurney, W. S., Hay, S. J., Head, E. J., et al. (2004). Comparative ecology of overwintering *Calanus finmarchicus* in the northern North Atlantic, and implications for life-cycle patterns. *ICES Journal of Marine Science*, *61*(4), 698–708. https://doi.org/10.1016/J.ICESJMS.2004.03.013

Helland-Hansen, B., & Nansen, F. (1909). The Norwegian Sea: Its physical oceanography based upon the Norwegian research 1900–1904. *Report on Norwegian Fishery and Marine Investigations*, *2*, 1–360.

Herman, A. W. (1992). Design and calibration of a new optical plankton counter capable of sizing small zooplankton. *Deep Sea Research Part A: Oceanographic Research Papers*, *39*(3–4), 395–415. https://doi.org/10.1016/0198-0149(92)90080-D

Herman, A. W., Beanlands, B., & Phillips, F. (2004). The next generation of optical plankton counter: The laser-OPC. *Journal of Plankton Research*, *26*(10), 1135–1145. https://doi.org/10.1093/PLANKT/FBH095

Hirche, H. J. (1996). Diapause in the marine copepod, *Calanus finmarchicus*–A review. *Ophelia*, *44*(1–3), 129–143. https://doi.org/10.1080/00785326.1995.10429843

Hu, Z. Y., & Zhou, M. (2019). Lagrangian analysis of surface transport patterns in the northern South China sea. *Deep Sea Research Part II: Topical Studies in Oceanography*, *167*, 4–13. https://doi.org/10.1016/J.DSR2.2019.06.020

Isachsen, P. E. (2015). Baroclinic instability and the mesoscale eddy field around the Lofoten Basin. *Journal of Geophysical Research: Oceans*, *120*(4), 2884–2903. https://doi.org/10.1002/2014JC010448

Ji, R., Ashjian, C. J., Campbell, R. G., Chen, C., Gao, G., Davis, C. S., et al. (2012). Life history and biogeography of *Calanus* copepods in the Arctic Ocean: An individual-based modeling study. *Progress in Oceanography*, *96*(1), 40–56. https://doi.org/10.1016/J.POCEAN.2011.10.001

Kang, D., & Curchitser, E. N. (2015). Energetics of eddy–mean flow interactions in the Gulf Stream region. *Journal of Physical Oceanography*, *45*(4), 1103–1120. https://doi.org/10.1175/JPO-D-14-0200.1

Krumhansl, K. A., Head, E. J. H., Pepin, P., Plourde, S., Record, N. R., Runge, J. A., & Johnson, C. L. (2018). Environmental drivers of vertical distribution in diapausing *Calanus* copepods in the Northwest Atlantic. *Progress in Oceanography*, *162*, 202–222. https://doi.org/10.1016/J.POCEAN.2018.02.018

Lehahn, Y., d'Ovidio, F., Lévy, M., & Heifetz, E. (2007). Stirring of the northeast Atlantic spring bloom: A Lagrangian analysis based on multisatellite data. *Journal of Geophysical Research*, *112*(C8), C08005. https://doi.org/10.1029/2006JC003927

Lévy, M., Franks, P. J. S., & Smith, K. S. (2018). The role of submesoscale currents in structuring marine ecosystems. *Nature Communications*, *9*(1), 4758. https://doi.org/10.1038/S41467-018-07059-3

Li, B., Zhou, L., Wang, C., Gao, C., Qin, J., & Meng, Z. (2020). Modulation of tropical cyclone genesis in the Bay of Bengal by the Central Indian Ocean Mode. *Journal of Geophysical Research: Atmospheres*, *125*(12), e2020JD032641. https://doi.org/10.1029/2020JD032641

Li, S., Zhang, Z., Zhou, M., Wang, C., Wu, H., & Zhong, Y. (2022). The role of fronts in horizontal transports of the Changjiang River plume in summer and the implications for phytoplankton blooms. *Journal of Geophysical Research: Oceans*, *127*(8), e2022JC018541. https://doi.org/10.1029/2022JC018541

Magalhães, F. C., Azevedo, J. L. L., & Oliveira, L. R. (2017). Energetics of eddy-mean flow interactions in the Brazil current between 20°S and 36°S. *Journal of Geophysical Research: Oceans*, *122*(8), 6129–6146. https://doi.org/10.1002/2016JC012609

Melle, W., Runge, J., Head, E., Plourde, S., Castellani, C., Licandro, P., et al. (2014). The North Atlantic Ocean as habitat for *Calanus finmarchicus*: Environmental factors and life history traits. *Progress in Oceanography*, *129*, 244–284. https://doi.org/10.1016/J.POCEAN.2014.04.026

Menna, M., & Poulain, P. M. (2014). Geostrophic currents and kinetic energies in the Black Sea estimated from merged drifter and satellite altimetry data. *Ocean Science*, *10*(2), 155–165. https://doi.org/10.5194/OS-10-155-2014

Olascoaga, M. J., Beron-Vera, F. J., Brand, L. E., & Kocak, H. (2008). Tracing the early development of harmful algal blooms on the West Florida Shelf with the aid of Lagrangian coherent structures. *Journal of Geophysical Research*, *113*(C12), C12014. https://doi.org/10.1029/2007JC004533

Opdal, A. F., & Vikebø, F. B. (2015). Long-term stability in modelled zooplankton influx could uphold major fish spawning grounds on the Norwegian continental shelf. *Canadian Journal of Fisheries and Aquatic Sciences*, *73*(2), 189–196. https://doi.org/10.1139/CJFAS-2014-0524

Pedersen, O. P., Tande, K. S., & Slagstad, D. (2001). A model study of demography and spatial distribution of *Calanus finmarchicus* at the Norwegian coast. *Deep Sea Research Part II: Tropical Studies in Oceanography*, *48*(1–3), 567–587. https://doi.org/10.1016/S0967-0645(00)00127-2

Planque, B. (2000). *Calanus finmarchicus* in the North Atlantic: The year of *Calanus* in the context of interdecadal change. *ICES Journal of Marine Science*, *57*(6), 1528–1535. https://doi.org/10.1006/JMSC.2000.0970

Raj, R. P., Johannessen, J. A., Eldevik, T., Nilsen, J. E. Ø., & Halo, I. (2016). Quantifying mesoscale eddies in the Lofoten Basin. *Journal of Geophysical Research: Oceans*, *121*(7), 4503–4521. https://doi.org/10.1002/2016JC011637

Rypina, I. I., Kamenkovich, I., Berloff, P., & Pratt, L. (2012). Eddy-induced particle dispersion in the near-surface. *Journal of Physical Oceanography*, *42*(12), 2206–2228. https://doi.org/10.1175/JPO-D-11-0191.1

Sætre, R. (1999). Features of the central Norwegian shelf circulation. *Continental Shelf Research*, *19*(14), 1809–1831. https://doi.org/10.1016/S0278-4343(99)00041-2

Saumweber, W. J., & Durbin, E. G. (2006). Estimating potential diapause duration in *Calanus finmarchicus*. *Deep Sea Research Part II: Tropical Studies of Oceanography*, *53*(23–24), 2597–2617. https://doi.org/10.1016/J.DSR2.2006.08.003

Scales, K. L., Hazen, E. L., Jacox, M. G., Castruccio, F., Maxwell, S. M., Lewison, R. L., & Bograd, S. J. (2018). Fisheries bycatch risk to marine megafauna is intensified in Lagrangian coherent structures. *Proceedings of the National Academy of Sciences of the United States of America*, *115*(28), 7362–7367. https://doi.org/10.1073/PNAS.1801270115

Sgubin, G., Swingedouw, D., Drijfhout, S., Mary, Y., & Bennabi, A. (2017). Abrupt cooling over the North Atlantic in modern climate models. *Nature Communications*, *8*(1), 14375. https://doi.org/10.1038/NCOMMS14375

Skagseth, Ø., Drinkwater, K. F., & Terrile, E. (2011). Wind- and buoyancy-induced transport of the Norwegian coastal current in the Barents Sea. *Journal of Geophysical Research*, *116*(C8), C08007. https://doi.org/10.1029/2011JC006996

Slagstad, D. L., & Tande, K. S. (1996). The importance of seasonal vertical migration in across shelf transport of *Calanus finmarchicus*. *Ophelia*, *44*(1–3), 189–205. https://doi.org/10.1080/00785326.1995.10429847

Slagstad, D. L., & Tande, K. S. (2007). Structure and resilience of overwintering habitats of *Calanus finmarchicus* in the Eastern Norwegian Sea. *Deep Sea Research Part II: Tropical Studies of Oceanography*, *54*(23–26), 2702–2715. https://doi.org/10.1016/J.DSR2.2007.08.024

Søiland, H., Chafik, L., & Rossby, T. (2016). On the long-term stability of the Lofoten Basin Eddy. *Journal of Geophysical Research: Oceans*, *121*(7), 4438–4449. https://doi.org/10.1002/2016JC011726

Søiland, H., & Rossby, T. (2013). On the structure of the Lofoten Basin Eddy. *Journal of Geophysical Research: Oceans*, *118*(9), 4201–4212. https://doi.org/10.1002/JGRC.20301

Sundby, S. (1984). Influence of bottom topography on the circulation at the continental shelf off northern Norway. *Fiskeridirektoratets Skrifter Serie Havundersokelser*, *17*, 501–519.

Tew Kai, E., Rossi, V., Sudre, J., Weimerskirch, H., Lopez, C., Hernandez-Garcia, E., et al. (2009). Top marine predators track Lagrangian coherent structures. *Proceedings of the National Academy of Sciences of the United States of America*, *106*(20), 8245–8250. https://doi.org/10.1073/PNAS.0811034106

Trodahl, M., & Isachsen, P. E. (2018). Topographic influence on baroclinic instability and the mesoscale eddy field in the northern North Atlantic Ocean and the Nordic seas. *Journal of Physical Oceanography*, *48*(11), 2593–2607. https://doi.org/10.1175/JPO-D-17-0220.1

Våge, S., Basedow, S. L., Tande, K. S., & Zhou, M. (2014). Physical structure of the Barents Sea Polar Front near Storbanken in August 2007. *Journal of Marine Systems*, *130*, 256–262. https://doi.org/10.1016/J.JMARSYS.2011.11.019

Verezemskaya, P., Barnier, B., Gulev, S. K., Gladyshev, S., Molines, J.-M., Gladyshev, V., et al. (2021). Assessing eddying (1/12°) ocean reanalysis GLORYS12 using the 14-yr instrumental record from 59.5°N section in the Atlantic. *Journal of Geophysical Research: Oceans*, *126*(6), e2020JC016317. https://doi.org/10.1029/2020JC016317

Visser, A. W., & Jónasdóttir, S. H. (1999). Lipids and the seasonal vertical migration of *Calanus finmarchicus*. *Fisheries Oceanography*, *8*, 100–106. https://doi.org/10.1046/J.1365-2419.1999.00001.X

Weidberg, N., & Basedow, S. L. (2019). Long-term variability in overwintering copepod populations in the Lofoten Basin: The role of the North Atlantic oscillation and trophic effects. *Limnology & Oceanography*, *64*(5), 2044–2058. https://doi.org/10.1002/LNO.11168

Weidberg, N., Hernandeza, N. S., Renner, A. H. H., & Basedow, S. L. (2022). Large scale patches of *Calanus finmarchicus* and associated hydrographic conditions off the Lofoten archipelago. *Journal of Marine Systems*, *227*, 103697. https://doi.org/10.1016/J.JMARSYS.2021.103697

Yan, X., Kang, D., Curchitser, E. N., & Pang, C. (2019). Energetics of eddy-mean flow interactions along the western boundary currents in the North Pacific. *Journal of Physical Oceanography*, *49*(3), 789–810. https://doi.org/10.1175/JPO-D-18-0201.1

Yu, L.-S., Bosse, A., Fer, I., Orvik, K. A., Bruvik, E. M., Hessevik, I., & Kvalsund, K. (2017). The Lofoten Basin eddy: Three years of evolution as observed by Seagliders. *Journal of Geophysical Research: Oceans*, *122*(8), 6814–6834. https://doi.org/10.1002/2017JC012982

Zhang, Z., Wang, W., & Qiu, B. (2014). Oceanic mass transport by mesoscale eddies. *Science*, *345*(6194), 322–324. https://doi.org/10.1126/SCIENCE.1252418

Zhou, M., Tande, K. S., Zhu, Y., & Basedow, S. (2009). Productivity, trophic levels and size spectra of zooplankton in northern Norwegian shelf regions. *Deep Sea Research Part II: Tropical Studies in Oceanography*, *56*(21–22), 1934–1944. https://doi.org/10.1016/J.DSR2.2008.11.018

Zhu, Y., Tande, K. S., & Zhou, M. (2009). Mesoscale physical processes and zooplankton transport-retention in the northern Norwegian shelf region. *Deep Sea Research Part II: Tropical Studies in Oceanography*, *56*(21–22), 1922–1933. https://doi.org/10.1016/J.DSR2.2008